

Sub-10 ps time tagging of electromagnetic showers with scintillating glasses and SiPMs

Marco T. Lucchini^{1,2a}, Andrea Benaglia^{3a}, Stefan Gundacker^{4a}, Jack Illare^b, Paul Lecoq^a, Alfred A. Margaryan^b, Ashot A. Margaryan^b, Kristof Pauwels^{5a}, Etiennette Auffray^a

^aCERN, European Center for Nuclear Research, Esplanade des Particules, 1, Geneva, CH-1217, Switzerland

^bAFO Research Inc., P.O. Box 1934, Glendale, 91209, California, USA

Abstract

The high energy physics community has recently identified an e^+e^- Higgs factory as one of the next-generation collider experiments, following the completion of the High Luminosity LHC program at CERN. The moderate radiation levels expected at such colliders compared to hadron colliders, enables the use of less radiation tolerant but cheaper technologies for the construction of the particle detectors. This opportunity has triggered a renewed interest in the development of scintillating glasses for the instrumentation of large detector volumes such as homogeneous calorimeters. While the performance of such scintillators remains typically inferior in terms of light yield and radiation tolerance compared to that of many scintillating crystals, substantial progress has been made over the recent years. In this paper we have studied the time resolution of cerium-doped Alkali Free Fluorophosphate glasses using 150 GeV pions and at different depths of an electromagnetic shower produced from a 100 GeV electron beam at the CERN SPS H2 beam line. A single sensor time resolution of 14.4 ps and 5-7 ps was measured respectively in the two cases. With such a performance the present technology has the potential to address an emerging requirement of future detectors at collider experiments: measuring the time-of-flight of single charged particles as well as that of neutral particles showering inside the calorimeter and the time development of showers.

Keywords: Scintillating glasses, SiPMs, Time resolution, Timing detectors, Calorimeters, Future collider experiments

1. Introduction

For instrumentation of large detector volumes as those required for future particle collider experiments (such as the Future Circular Collider [1] at CERN, the Circular Electron Positron Collider in China [2], the International Linear Collider [3], the Cool Copper Collider, C³ [4] or the Electron Ion Collider [5]), scintillating heavy glasses have been considered since a long time as a cost-effective alternative to scintillating crystals. Beside relying on well developed production methods from the glass industry, the relatively low temperatures and less expensive raw materials required for the production of such scintillators make their manufacturing process simpler and cheaper compared to single crystals.

The latest update of the European Strategy for Particle Physics [6] has recently identified an electron-positron (e^+e^-) Higgs factory as one of the highest priorities in the mid-term future of particle accelerators. In such colliders the radiation levels will be lower by several order of magnitudes compared to the Large Hadron Collider (LHC), currently operating at CERN in the Geneva area, and also of its forthcoming high luminosity upgrade (HL-LHC). The requirements on the radiation tolerance of the scintillators are thus more relaxed and can be more

easily met by a wider spectrum of technologies. In this context, glass scintillators are often considered potential candidates for the instrumentation of homogeneous hadron calorimeters [7, 8] which require volumes as large as tens of cubic meters for which the cost of inorganic scintillators is a potential limiting factor. Glass scintillators could also be exploited in sampling calorimeters where their combination with a heavy absorber, such as tungsten or lead, can decrease the effective radiation length and Molière radius of the calorimeter [9, 10]. Scintillating glasses are for instance considered as an alternative to lead tungstate in an electromagnetic calorimeter for the Electron Ion Collider (EIC) [5] at the Brookhaven National Laboratory (BNL).

First tests on scintillating glasses for high energy physics applications date back to the 90's [11, 12] where they were initially considered as a possible alternative to lead tungstate crystals for instrumentation of the CMS electromagnetic calorimeter (but discarded because of insufficient radiation tolerance). In particular, hafnium fluoride scintillating glasses were also demonstrated capable to achieve a density up to 6.0 g/cm³ [13, 14]. More recently, new materials, such as cerium-doped barium silica glasses (DSB) [15, 16], cerium-doped Ba-Gd silica glasses (GDS) [17] and aluminoborosilicate glasses [18] have been developed showing enhanced light output and radiation tolerance.

While the performance of scintillating glasses remains inferior compared to other inorganic scintillators, (in terms of radiation tolerance, light output and stopping power) they can still

¹Corresponding author: marco.lucchini@unimib.it

²Now at INFN & University of Milano-Bicocca, Milano, Italy

³Now at INFN, Sez. Milano-Bicocca, Milano, Italy

⁴Now at RWTH Aachen University, Aachen, Germany.

⁵Now at ESRF: The European Synchrotron, Grenoble, France.

offer a cost-effective solution where such constraints are less demanding with a cost in the ballpark of 1 $\$/\text{cm}^3$.

Beside the usual requirement on the calorimeter energy resolution, in the context of future collider experiments a novel detector feature is often required: the capability to embed timing measurements of single charged tracks (MIPs) for time-of-flight measurements with dedicated timing layers [19, 20] as well as measuring accurately the time development of electromagnetic and hadronic showers inside the calorimeters [21, 22].

In this paper we present the results of a test beam campaign carried out in 2016 at the CERN H2 beam line, in which samples of dense scintillating Alkali Free Fluorophosphate glasses produced by AFO Research Inc. [23] have been exposed to a beam of pions and electrons. The performance of such scintillators, read-out with silicon photo-multipliers has been characterized in terms of time resolution for single charged track and at different positions along the longitudinal development of an electromagnetic shower.

2. Description of the test samples

A batch of Alkali Free Fluorophosphate glasses $\text{Al}(\text{PO}_3)_3\text{-Ba}(\text{PO}_3)_2\text{-BaF}_2\text{-MgF}_2$ (FP2035) doped with cerium were prepared with the highest purity chemicals. The batch was thoroughly mixed to achieve the required homogeneity and melted using a vitreous carbon crucible in an Ar atmosphere and underwent a special annealing process at various temperatures for 8 to 10 hours.

The presence of $\text{BaF}_2 + \text{MgF}_2$ effectively increases the chemical durability of these glasses. The glasses are chemically and physically stable and do not require any special handling. The combination of Fluorides and Phosphates in AFO glasses further enhances their overall physical, chemical, optical and radiation resistance performance [24].

In particular, the Alkali Free Fluorophosphate glasses used in this study contain up to 80% fluoride which has the highest electronegativity of 4 eV. The function of the cerium dopant in the glass matrix is dual: it improves the radiation resistance and acts as a scintillating agent [25].

A set of 1 cm^3 cubic samples with density of about 4.5 g/cm^3 and different cerium concentrations have been characterized at CERN. All samples were cut to dimensions of $10 \times 10 \times 10\text{ mm}^3$ with the six faces of the samples polished to a degree of optical quality. The list of samples is reported in Table 1 and a picture is shown in Fig. 1.

3. Characterization of optical and scintillation properties

The characteristic emission/excitation spectra and the transparency of the samples were measured in the laboratory with a dedicated Perkin Elmer LS 55 luminescence spectrometer and a Perkin Elmer Lambda 650 UV/VIS spectrometer respectively. All samples featured a characteristic emission wavelength peaking at 370 nm and a transmission cut-off wavelength around 340 nm with a small shift towards higher wavelength depending on the cerium content. They also show a broad excitation

Table 1: List of glass samples tested with different cerium concentrations.

Sample ID	Dimensions [mm^3]	Cerium content [%]
3105	$10 \times 10 \times 10$	0.5
3102	$10 \times 10 \times 10$	1.0
3145	$10 \times 10 \times 10$	1.5
3147	$10 \times 10 \times 10$	2.0
3149	$10 \times 10 \times 10$	2.5
3151	$10 \times 10 \times 10$	3.0
3152	$10 \times 10 \times 10$	5.0
3153	$10 \times 10 \times 10$	5.0



Figure 1: Picture of two cubic $10 \times 10 \times 10\text{ mm}^3$ glass samples.

continuum in the 200-300 nm range with a peak value around 330 nm. An example of the measured spectra is shown in Fig. 2 for the sample with 5% cerium content.

The decay time of the scintillation was also evaluated with a time correlated single photon counting method as described in [26] and revealed a dominant (93%) decay time constant of about 42 ns and a small (7%) fast component of about 4 ns as reported in Fig. 3. An effective decay time was defined as the harmonic sum of the two components:

$$\tau_{eff} = \left(\frac{I_1}{\tau_1} + \frac{I_2}{\tau_2} \right)^{-1} \quad (1)$$

in which I_i are the relative light yields (normalized to area) of the decay time components τ_i with $\sum_i I_i = 1$. It was observed that τ_{eff} varied from about 31 ns (for the sample with 1.5% cerium content) down to 27 ns for the sample with 5.0% cerium content.

When wrapped with Teflon and coupled with optical grease ($n=1.45$) to a Photonics R2059 photomultiplier tube a light output ranging from 200 to 700 photons/MeV (depending on the cerium content) was measured using a ^{137}Cs source. A typical spectrum of the integrated charge, calibrated in number of photoelectrons, and the dependence of the light output as a function of the cerium content are reported in Fig. 4. These scintillation properties are in agreement with previous measurements performed on similar samples [27].

Given their higher light output and faster decay time, AFO glasses with a cerium content of 5% have been selected for testing with high energy beams, as described in the following section.

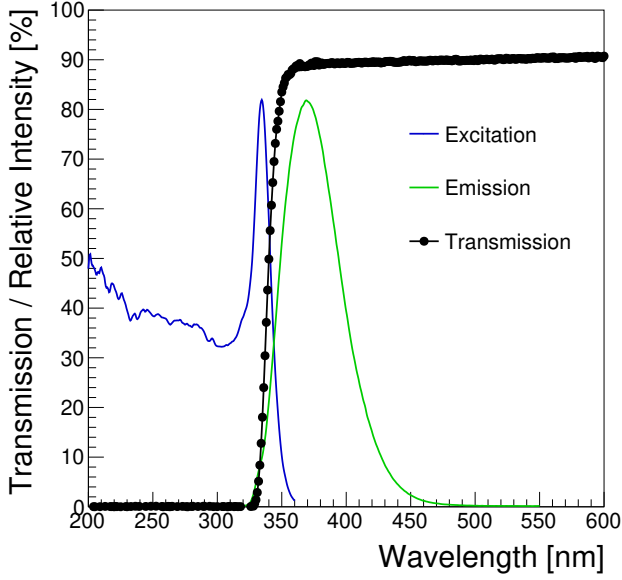


Figure 2: Excitation (blue line), emission (green line) and transmission (black dots) spectra measured on a AFO glass sample with 5% of cerium content.

4. Test beam experimental setup and methods

The scintillating samples have been wrapped with several layers of Teflon except on one face which was coupled using Meltmount glue to a Silicon Photomultiplier (SiPM). A pair of $3 \times 3 \times 10 \text{ mm}^3$ LYSO:Ce crystals produced by Crystal Photonics (CPI), coupled with $3 \times 3 \text{ mm}^2$ TSV Hamamatsu (HPK) SiPMs ($50 \mu\text{m}$ cell size), was placed in front of the glass samples under test as a reference detector. The scintillating glass samples of $10 \times 10 \times 10 \text{ mm}^3$ were coupled to HPK S13360-6050PE SiPMs with a larger active area of $6 \times 6 \text{ mm}^2$ to increase the light collection efficiency. The SiPMs were readout with a custom board featuring the NINO chip for time discrimination and a parallel output for the readout of the signal amplitude [28].

The experimental configurations and readout scheme are summarized in Fig. 5 and Fig. 6. The scintillators, the SiPMs and the electronic boards were housed in a light tight box with a water cooled system to maintain a temperature stable at $18 \pm 1^\circ\text{C}$. A picture of the actual setup inside the box is reported in Fig. 7.

Both the analog SiPM amplitude and the digital output from the NINO chip were digitized at 5 GS/s using a Caen V1742 module. The amplitude of each crystal was reconstructed as the maximum of the analog pulse, whereas the time was computed at the 50% of the NINO output amplitude and extracted from a linear fit of the signal leading edge. Since the NINO acts as fixed threshold discriminator a correction for amplitude walk is applied based on the signal analog amplitude. A detailed description of the experimental setup and data analysis procedure can be found in [29]. The noise of the readout electronics adds an intrinsic time jitter due to the ratio

$$\sigma_{t,el.noise} = \frac{\sigma_V}{dV/dt} \quad (2)$$

where σ_V is the electronic noise (fluctuations in the digitized signal due to electronic noise), mainly due to the Caen V1742 digitizer, and dV/dt is the measured rising slope of the output digital signal at the set 50% NINO threshold. The contribution from Eq. 2 was experimentally measured to be 4.2 ps/channel by splitting the same digital signal into two different channels of the digitizer and measuring the standard deviation of the difference between the two time stamps divided by $\sqrt{2}$.

The tests have been performed at the H2 beam line of CERN SPS North Area facility where pion and electron beams of respectively 150 GeV and 100 GeV energy were used. Pions have a small probability to start showering inside the test samples and thus mainly travel in a straight line through the samples depositing an energy through ionization similar to minimum ionizing particles (MIPs). Because of their different density and atomic composition, about 0.86 MeV/mm are deposited in LYSO:Ce crystals while 0.53 MeV/mm inside the AFO glasses, according to Geant4 simulations [30].

Conversely, electrons have a larger probability to start showering inside the test samples and have thus been used to test the performance of the glasses to detect an electromagnetic shower. A set of different copper blocks, placed in front of the glass samples, were used to study the response of the scintillators at different depths of an electromagnetic shower, in particular after 1, 3, 7 and 11 radiation lengths (X_0).

5. Results

5.1. Time resolution for single charged tracks

As a first step in the characterization of the test samples the time resolution for tagging single MIPs was estimated using a 150 GeV pion beam. The two glass samples of $10 \times 10 \times 10 \text{ mm}^3$ were coupled to $6 \times 6 \text{ mm}^2$ HPK SiPMs, operating at a bias voltage of 60 V corresponding to an over-voltage of about 6 V and thus with a photon detecting efficiency (PDE) of about 55% [31]. Events were selected by requiring a MIP-like signal in the two reference LYSO crystals located upstream. A typical spectrum of the signal amplitude before (black) and after the selection (green) is reported in the left panel of Fig. 8 featuring a landau distribution with most probable value around 6 mV. Two identical glass samples were placed one after the other and the time difference between the time stamps generated by the two samples is calculated. A typical distribution of such time difference is reported in the right panel of Fig. 8 before (black) and after applying amplitude walk corrections (blue). The time resolution of a single device can be estimated as the standard deviation of such Gaussian distribution divided by $\sqrt{2}$:

$$\sigma_{t,single}^{MIP} = \frac{\sigma_{CTR}}{\sqrt{2}} = \frac{20.4}{\sqrt{2}} = 14.4 \text{ ps} \quad (3)$$

5.2. Time resolution for electromagnetic showers

After qualification using the pion beam, a test using 100 GeV electrons has been performed. In this case, there is a non negligible probability for an electron to start showering already in the reference LYSO crystals which amounts to about 1.8 X_0 .

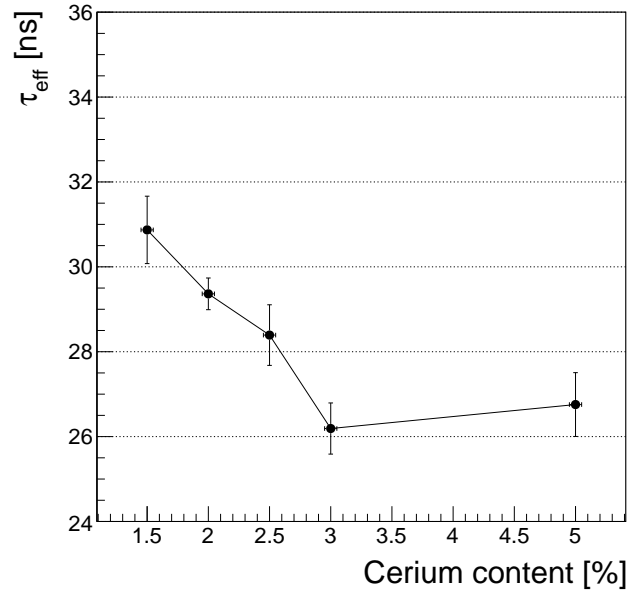
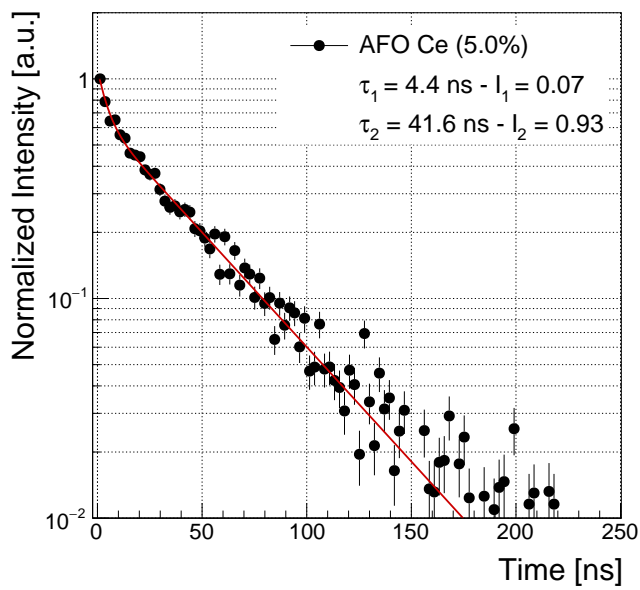


Figure 3: Left: scintillation decay time of AFO glass sample with 5% of cerium content measured with time correlated single photon counting method. The red line shows a fit of the distribution with a double exponential function used to assess the decay time components and their relative intensity as reported in the inset of the figure. Right: the effective decay time, τ_{eff} , of different samples is shown as a function of the cerium content.

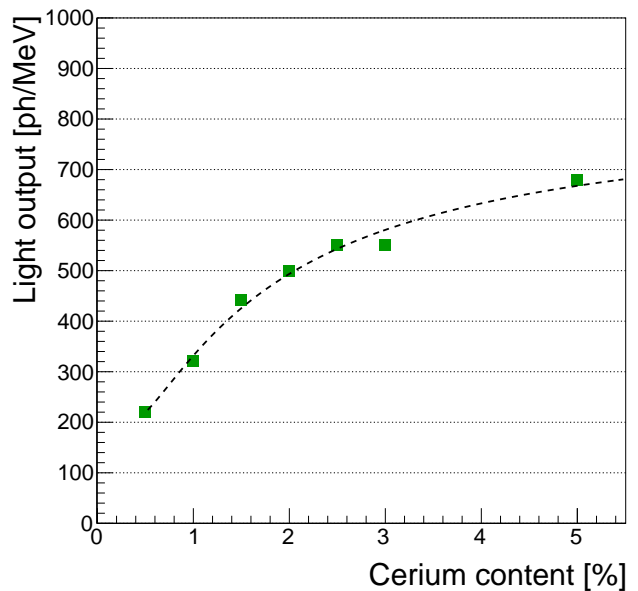
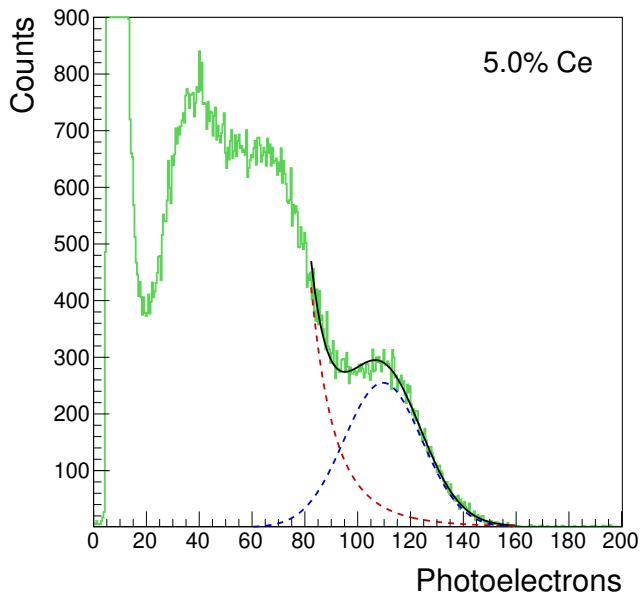


Figure 4: Left: example of the integrated charge calibrated spectrum obtained using a ^{137}Cs source for excitation of the glass sample with 5% cerium content. A fit of the spectrum with the sum of a polynomial and a Gaussian functions (describing the Compton shoulder and photoelectric peak resp.) is performed to evaluate the position of photo-peak. Right: the light output of the AFO glass samples is shown as a function of the cerium concentration. The black line is the result of an empirical fit with a function $f(x) = A - B * \exp(C/x)$ to emphasize the observed trend.

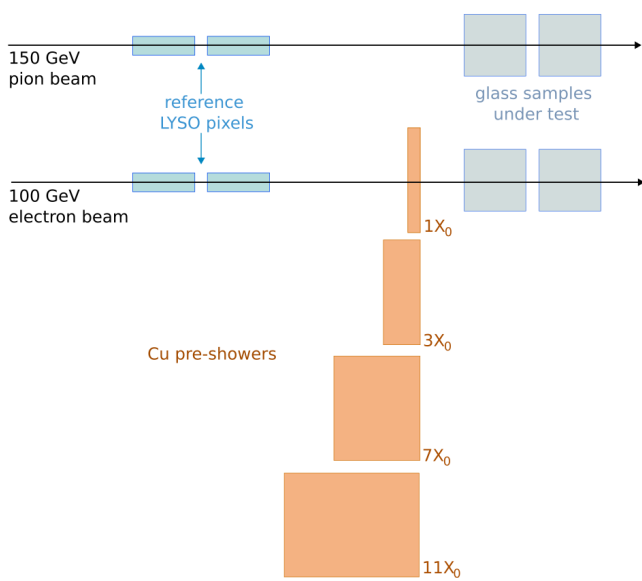


Figure 5: Sketch of the experimental configuration used for the testing of samples with pion beam and electromagnetic showers. Two reference LYSO crystals in front of the setup are used to tag the incoming particle, four different copper blocks of different thickness were placed in front of the two glass samples, on at a time.

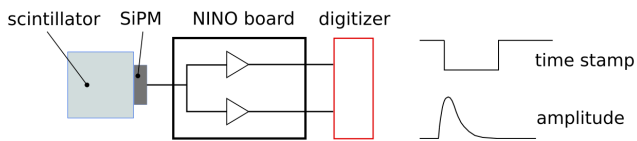


Figure 6: Signal detection and readout scheme: light is collected at the SiPMs which are readout with a custom electronic board featuring the NINO chip for time discrimination. Both a digital like signal from the discriminator and an analog waveform whose amplitude is proportional to the detected light signal are read out using a CAEN V1742 digitizer.

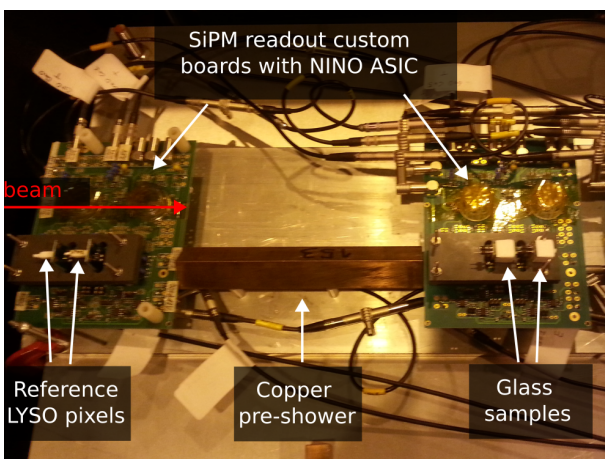


Figure 7: Picture of the experimental setup. Two electronic boards are used respectively for the readout of the LYSO reference crystals and the glass samples and are placed inside a light tight cooled box. A copper block of $11 X_0$ is placed in front of the glass samples.

In addition, different thicknesses of copper pre-shower blocks were placed between the reference samples and the glass samples under test to characterize the sensor response at different locations along the longitudinal development of the electromagnetic shower. The distance from the end of the absorber block and the first glass sample was about 2.0 cm thus allowing for some widening of the electromagnetic shower in air. The distribution of the maximum amplitudes observed (after requiring a MIP signal in the upstream reference LYSO sensors) are shown in the left panel of Fig. 9. The distributions are rather broad due to event-by-event fluctuations in the fraction of electromagnetic shower sampled by the active volume of the sensors.

As expected, the highest average signal is observed when the longitudinal development of the electromagnetic shower reaches its maximum around $6 X_0$ as shown in the right panel of Fig. 9. Since 1 cm of AFO glass corresponds to about $0.34 X_0$, there is a small shift in the longitudinal shower profiles observed by the two samples due to the additional material budget of the upstream sample.

Nevertheless, the average energy deposited in the two samples is very similar and we can approximately evaluate the time resolution of each single sensor from the time difference between the two identical glasses as described in Sec. 5.1 for the pions. The time resolution can be estimated as a function of the amount of material budget in front of the first samples, thus as a function of the depth of the electromagnetic shower longitudinal development. After a few radiation lengths the time resolution becomes better than 10 ps and reaches an optimal value of about 7 ps at the shower maximum, in correspondence of the highest signal, as shown in Fig. 10.

Since the amount of energy deposited in the glass samples features a broad distribution it is convenient to parameterize the time resolution as a function of the signal amplitude. To do so, all events taken at different depths of the shower longitudinal development have been used. Events are then subdivided in intervals of 10 mV width based on the average signal amplitude of the two sensors, $\langle \text{amp.} \rangle = (\text{amp}_{\text{ch1}} + \text{amp}_{\text{ch2}})/2$ as illustrated in the left panel of Fig. 11. For the events inside each amplitude interval the time resolution is then estimated from a Gaussian fit of the time difference distributions shown in the right panel of Fig. 11. A few amplitude intervals in the range 35-95 mV, where an improvement in time resolution is observed, have been highlighted with different colors in both figures for illustrative purposes.

The time resolution as a function of signal amplitude is shown in Fig. 12 both with (black dots) and without (blue dots) applying amplitude walk corrections. In addition, the contribution from the digitizer electronic noise was subtracted in quadrature to evaluate the contribution to the time resolution originating from the sensor (scintillator and SiPM). For signals with amplitudes larger than 70 mV (roughly corresponding to about 12 MIPs based on the sensor response to single pions) a time resolution between 5 and 6 ps is obtained. A constant term of about 5 ps is reached for amplitudes larger than 80 mV, and could be attributed either to the electronic noise at the discriminator input in the NINO ASIC or to other sources of time jitter intrinsic to the stochastic nature of electromagnetic showers.

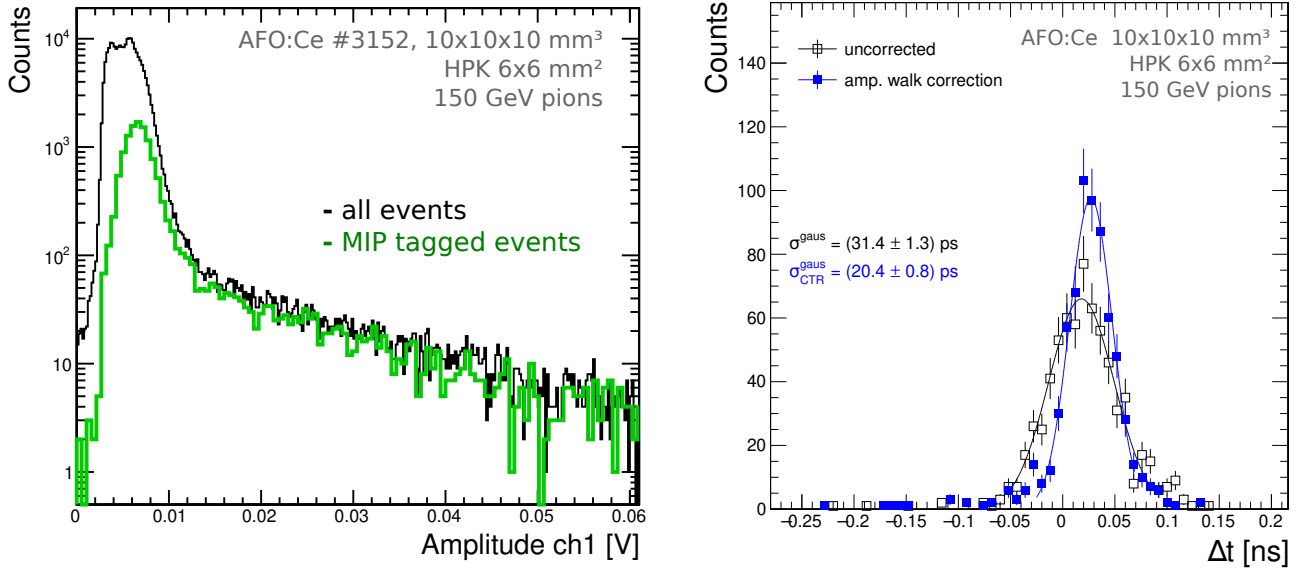


Figure 8: Left: Distribution of the signal amplitude measured from the pair of AFO:Ce glasses with 5% cerium content in response to 150 GeV pion beam. The green distribution represents the events in which a MIPs was tagged using the reference LYSO crystals located upstream and which have thus been selected to compute the time resolution. Right: Coincidence time resolution for AFO:Ce glasses with 5% cerium content for detection of single pions with (blue squares) and without (black empty dots) amplitude walk correction.

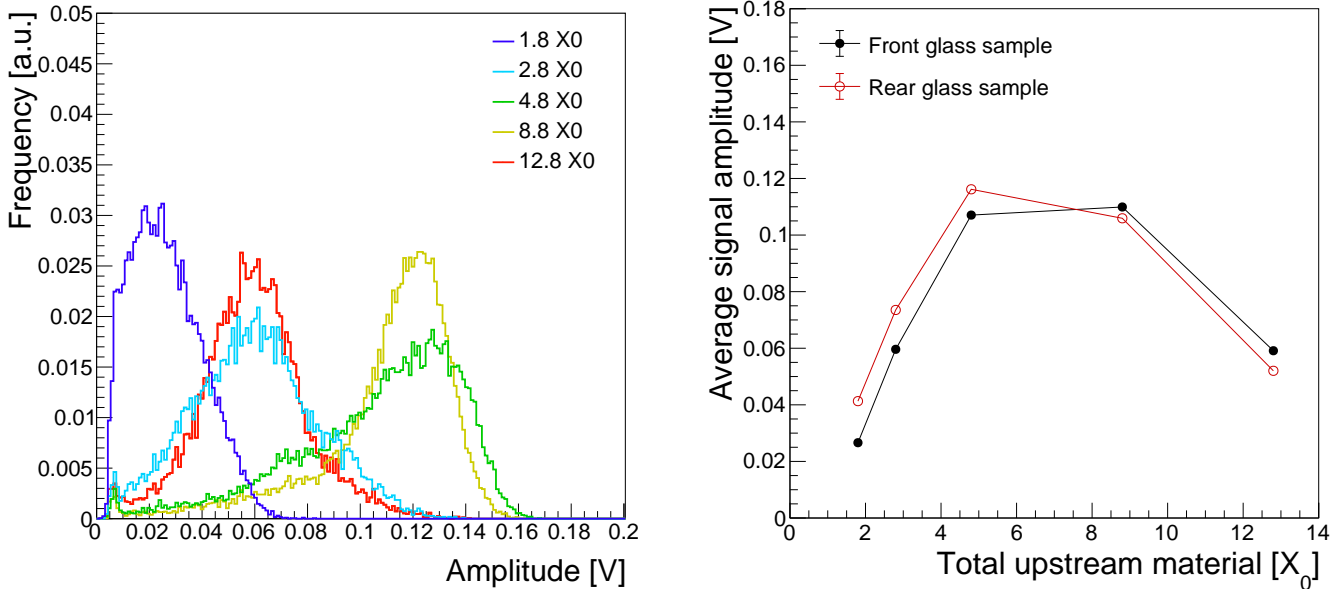


Figure 9: Left: Amplitude spectra of the upstream glass sample for different thicknesses of pre-showers copper blocks located in front of the sample. Right: Average signal amplitude for the front (black full dots) and rear (red empty dots) glass samples as a function of the total amount of material placed in front of the sample (LYSO reference crystals and copper block), expressed in equivalent radiation lengths, X_0 .

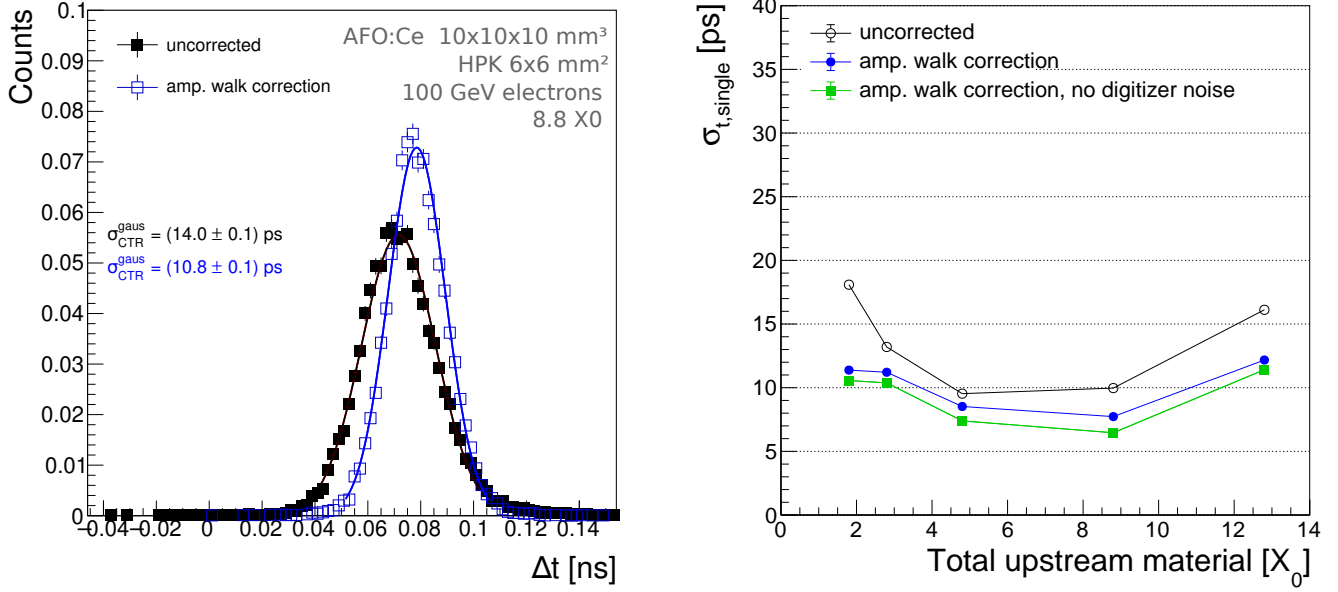


Figure 10: Left: Coincidence time resolution for AFO:Ce glasses with 5% cerium content for detection of 100 GeV electron showers after 8.8 X₀ of upstream material, with (blue squares) and without (black empty dots) amplitude walk correction. Right: Time resolution of a single glass+SiPM sensor as a function of the total amount of material (LYSO reference crystals and copper block) located in front of the glass samples. The black dots represent the time resolution before amplitude walk corrections, blue after amplitude walk corrections and green is the time resolution of the devices after subtracting in quadrature the contribution from the CAEN V1742 digitizer electronic noise.

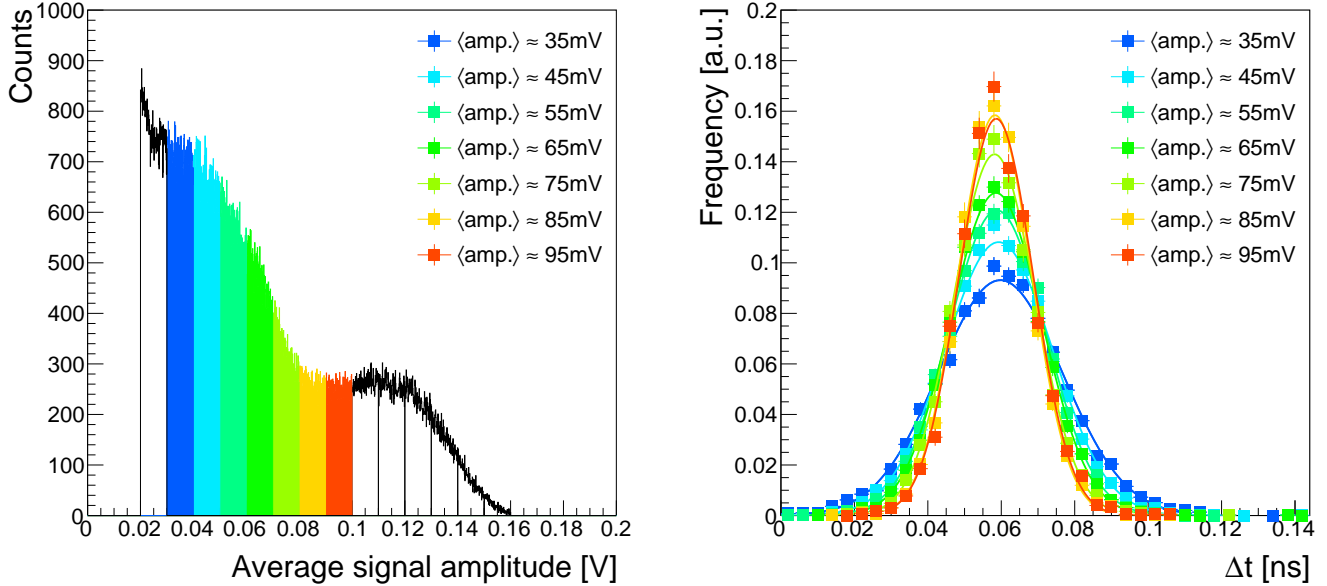


Figure 11: Left: Cumulative distribution of the average signal amplitude for 100 GeV electrons obtained by merging together all events, taken using different thicknesses of the Cu pre-shower. The entire distribution is divided in intervals of 10 mV width. For illustrative purpose a few bins have been highlighted with colors. Right: the distribution of time differences between the two glass samples, after amplitude walk corrections, are shown in the right panel corresponding to the same intervals of amplitude highlighted with the same colors in the left figure.

6. Conclusions

The time resolution of sensors made of 1 cm³ scintillating heavy glass (cerium-doped Alkali Free Fluorophosphates) cou-

pled with SiPMs has been characterized using high energy particle beams from the CERN H2 beam line. A single device time resolution of about 14 ps was measured for tagging of single

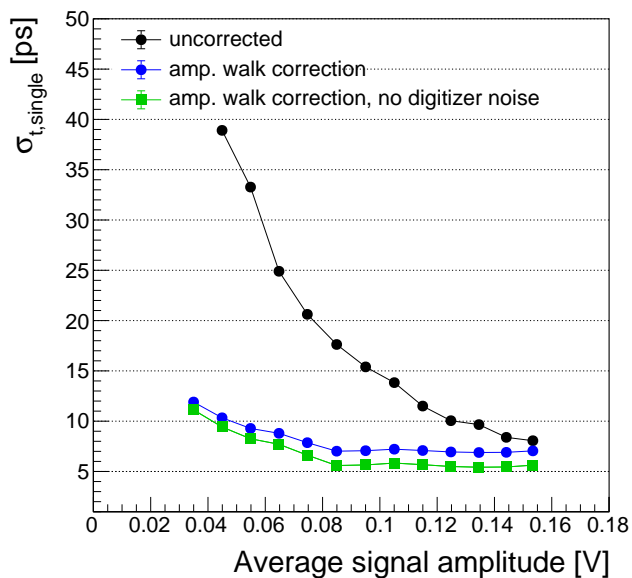


Figure 12: Single device time resolution as a function of the average signal amplitude of the two glass samples. The time resolution is shown before amplitude walk corrections (black dots) and after (blue dots). The green squares curve represent the intrinsic time resolution of the glass+SiPM detector after subtracting the contribution from the data acquisition system (i.e. from the CAEN digitizer noise).

pion events (MIP-like) while a resolution in the range between 6 and 12 ps was achieved in measuring the core of electromagnetic showers at longitudinal depths between 3 and 12 X_0 . The present results encourage the potential use of similar technologies to address an emerging requirement for particle detectors at future collider experiments, i.e. the development of a dedicated timing layer for measurements of the time-of-flight of charged particles or for measuring the time development of electromagnetic and hadronic showers inside calorimeters.

Acknowledgement

This work was performed in the framework of the Crystal Clear Collaboration and received funding from the European Research Council under the European Union’s Seventh Framework Programme (FP/2007–2013) under ERC Grant Agreement n. 338953-TICAL and under Grant Agreement 289355-PicoSEC-MCNet. Support has been received also from the COST Action (TD1401, FAST), supported by COST (European Cooperation in Science and Technology). We also acknowledge the support received from the CERN SPS facility experts which made these measurements possible.

References

- [1] M. Benedikt, et al., Future Circular Collider, Tech. Rep. CERN-ACC-2018-0057, CERN, Geneva, published in Eur. Phys. J. ST. (Dec 2018). URL <http://cds.cern.ch/record/2651299>
- [2] The CEPC Study Group, CEPC conceptual design report: Volume 1 - accelerator (2018). arXiv:1809.00285. URL <https://arxiv.org/abs/1809.00285>

- [3] ILC Collaboration, The ILC Technical Design Report (Jun 2013). URL <http://www.linearcollider.org/ILC/Publications/Technical-Design-Report>
- [4] S. Dasu, et al., Strategy for understanding the higgs physics: The cool copper collider (2022). doi:10.48550/ARXIV.2203.07646. URL <https://arxiv.org/abs/2203.07646>
- [5] F. Willeke, J. Beebe-Wang, Electron ion collider conceptual design report 2021 (2 2021). doi:10.2172/1765663. URL <https://www.osti.gov/biblio/1765663>
- [6] The European Strategy Group, Deliberation document on the 2020 Update of the European Strategy for Particle Physics, CERN Council, Geneva, 2020. doi:10.17181/ESU2020Deliberation. URL <http://cds.cern.ch/record/2720131>
- [7] D. D. et al., Development of a novel highly granular hadronic calorimeter with scintillating glass tiles (2022). URL <https://indico.cern.ch/event/847884/contributions/4831420/>
- [8] R. Mao, L. Zhang, R.-Y. Zhu, Crystals for the HHCAL detector concept, Journal of Physics: Conference Series 404 (2012) 012029. doi:10.1088/1742-6596/404/1/012029. URL <https://doi.org/10.1088/1742-6596/404/1/012029>
- [9] D. Du, Y. Liu, Development of a novel highly granular hadronic calorimeter with scintillating glass tiles, Instruments 6 (3) (2022). doi:10.3390/instruments6030032. URL <https://www.mdpi.com/2410-390X/6/3/32>
- [10] V. Dormenev, A. Amelina, E. Auffray, K.-T. Brinkmann, G. Dosovitskiy, F. Cova, A. Fedorov, S. Gundacker, D. Kazlou, M. Korjik, N. Kratochwil, V. Ladygin, V. Mechinsky, M. Moritz, S. Nargelas, R. Novotny, P. Orsich, M. Salomoni, Y. Talochka, G. Tamulaitis, A. Vaitkevicius, A. Vedda, H.-G. Zaunick, Multipurpose ce-doped ba-gd silica glass scintillator for radiation measurements, Nuclear Instruments and Methods in Physics Research Section A: Accelerators, Spectrometers, Detectors and Associated Equipment 1015 (2021) 165762. doi:<https://doi.org/10.1016/j.nima.2021.165762>. URL <https://www.sciencedirect.com/science/article/pii/S0168900221007476>
- [11] E. Auffray, D. Bouttet, I. Dafinei, J. Fay, P. Lecoq, J. Mares, M. Martini, G. Mazé, F. Meinardi, B. Moine, M. Nikl, C. Pedrini, M. Poulain, M. Schneegans, S. Tavernier, A. Vedda, Cerium doped heavy metal fluoride glasses, a possible alternative for electromagnetic calorimetry, Nuclear Instruments and Methods in Physics Research Section A: Accelerators, Spectrometers, Detectors and Associated Equipment 380 (3) (1996) 524–536. doi:[https://doi.org/10.1016/0168-9002\(96\)00717-6](https://doi.org/10.1016/0168-9002(96)00717-6). URL <https://www.sciencedirect.com/science/article/pii/S0168900296007176>
- [12] I. Dafinei, E. Auffray, P. Lecoq, et al., Heavy fluoride glasses as an alternative to crystals in high energy physics calorimetry, MRS Online Proceedings Library 348 (1994) 217–221. URL <https://doi.org/10.1557/PROC-348-217>
- [13] P. Hobson, D. Imrie, T. Price, S. Sheikh, K. Bell, R. Brown, D. Cockerill, P. Flower, G. Grayer, B. Kennedy, A. Lintern, P. Jeffreys, M. Sproston, K. McKinlay, J. Parker, D. Bowen, T. Cliff, R. Stewart-Hannay, R. Hammond-Smith, The development of dense scintillating hafnium fluoride glasses for the construction of homogeneous calorimeters in particle physics, Journal of Non-Crystalline Solids 213-214 (1997) 147–151. doi:[https://doi.org/10.1016/S0022-3093\(96\)00664-3](https://doi.org/10.1016/S0022-3093(96)00664-3). URL <https://www.sciencedirect.com/science/article/pii/S0022309396006643>
- [14] S. Shaukat, K. McKinlay, P. Flower, P. Hobson, J. Parker, Optical and physical characteristics of hblan fluoride glasses containing cerium, Journal of Non-Crystalline Solids 244 (2) (1999) 197–204. doi:[https://doi.org/10.1016/S0022-3093\(99\)00020-4](https://doi.org/10.1016/S0022-3093(99)00020-4). URL <https://www.sciencedirect.com/science/article/pii/S0022309399000204>
- [15] E. Auffray, N. Akchurin, A. Benaglia, A. Borisevich, C. Cowden, J. Damgov, V. Dormenev, C. Dragoiu, P. Duderu, M. Korjik, D. Kozlov, S. Kunori, P. Lecoq, S. W. Lee, M. Lucchini, V. Mechinsky, K. Pauwels, DSB:ce scintillation glass for future, Journal of Physics: Conference Series 587 (2015) 012062. doi:10.1088/1742-6596/587/1/012062. URL <https://doi.org/10.1088/1742-6596/587/1/012062>

- [16] R. W. Novotny, K. T. Brinkmann, V. Dormenev, P. Drexler, M. Korjik, D. Kozlov, H. G. Zaunick, Performance of DSB - a new glass and glass ceramic as scintillation material for future calorimetry, *Journal of Physics: Conference Series* 1162 (2019) 012023. doi:10.1088/1742-6596/1162/1/012023. URL <https://doi.org/10.1088/1742-6596/1162/1/012023>
- [17] A. Amelina, A. Mikhlin, S. Belus, A. Bondarev, A. Borisevich, D. Kuznetsova, I. Komroto, V. Mechinsky, D. Kozlov, P. Volkov, G. Dosovitskiy, M. Korzhik, (gd,ce)2o3-al2o3-sio2 scintillation glass, *Journal of Non-Crystalline Solids* 580 (2022) 121393. doi:<https://doi.org/10.1016/j.jnoncrysol.2021.121393>. URL <https://www.sciencedirect.com/science/article/pii/S0022309321007201>
- [18] G. Tang, Z. Hua, S. Qian, X. Sun, H. Ban, H. Cai, S. Li, H. Liu, S. Liu, L. Ma, L. Qin, X. Sun, Z. Wang, Y. Wen, Q. Wu, Y. Zhu, L. Zhang, Optical and scintillation properties of aluminoborosilicate glass, *Optical Materials* 130 (2022) 112585. doi:<https://doi.org/10.1016/j.optmat.2022.112585>. URL <https://www.sciencedirect.com/science/article/pii/S092534672200619X>
- [19] CMS Collaboration, A MIP Timing Detector for the CMS Phase-2 Upgrade, Tech. Rep. CERN-LHCC-2019-003. CMS-TDR-020, CERN, Geneva (Mar 2019). URL <https://cds.cern.ch/record/2667167>
- [20] L. Gruber, S. Brunner, J. Marton, H. Orth, K. Suzuki, Barrel time-of-flight detector for the PANDA experiment at FAIR, *Nuclear Instruments and Methods in Physics Research Section A: Accelerators, Spectrometers, Detectors and Associated Equipment* 824 (2016) 104 – 105, *frontier Detectors for Frontier Physics: Proceedings of the 13th Pisa Meeting on Advanced Detectors*. doi:<https://doi.org/10.1016/j.nima.2015.10.108>. URL <http://www.sciencedirect.com/science/article/pii/S0168900215013479>
- [21] A. Benaglia, E. Auffray, P. Lecoq, H. Wenzel, A. Para, Space-time development of electromagnetic and hadronic showers and perspectives for novel calorimetric techniques, *IEEE Transactions on Nuclear Science* 63 (2) (2016) 574–579. doi:10.1109/TNS.2016.2527758.
- [22] N. Akchurin, C. Cowden, J. Damgov, A. Hussain, S. Kunori, On the use of neural networks for energy reconstruction in high-granularity calorimeters, *Journal of Instrumentation* 16 (12) (2021) P12036. doi:10.1088/1748-0221/16/12/p12036.
- [23] Afo research inc. (2022). URL <https://www.aforesearch.com/>
- [24] A. A. Margaryan, *Ligands and Modifiers in Vitreous Materials - The Spectroscopy of Condensed Systems*, World Scientific Publishing Co., Singapore, New Jersey, London, Hong Kong, 1999.
- [25] M. Lucchini, Scintillation properties and radiation tolerance of alkali free fluorophosphate glasses with different dopant concentrations (2017). URL <https://indico.cern.ch/event/388511/contributions/2612825/>
- [26] L. M. Bollinger, G. E. Thomas, Measurement of the time dependence of scintillation intensity by a delayed-coincidence method, *Review of Scientific Instruments* 32 (9) (1961) 1044–1050. doi:10.1063/1.1717610. URL <https://doi.org/10.1063/1.1717610>
- [27] C. Hu, A. Margaryan, A. Margaryan, F. Yang, L. Zhang, R.-Y. Zhu, Alkali-free ce-doped and co-doped fluorophosphate glasses for future hep experiments, *Nuclear Instruments and Methods in Physics Research Section A: Accelerators, Spectrometers, Detectors and Associated Equipment* 954 (2020) 161665, *symposium on Radiation Measurements and Applications XVII*. doi:<https://doi.org/10.1016/j.nima.2018.11.124>. URL <https://www.sciencedirect.com/science/article/pii/S0168900218317777>
- [28] S. Gundacker, E. Auffray, B. Frisch, P. Jarron, A. Knapitsch, T. Meyer, M. Pizzichemi, P. Lecoq, Time of flight positron emission tomography towards 100ps resolution with l(y)SO: an experimental and theoretical analysis, *Journal of Instrumentation* 8 (07) (2013) P07014–P07014. doi:10.1088/1748-0221/8/07/p07014. URL <https://doi.org/10.1088/1748-0221/8/07/p07014>
- [29] A. Benaglia, S. Gundacker, P. Lecoq, M. Lucchini, A. Para, K. Pauwels, E. Auffray, Detection of high energy muons with sub-20ps timing resolution using L(Y)SO crystals and SiPM readout, *Nuclear Instruments and Methods in Physics Research Section A: Accelerators, Spectrometers, Detectors and Associated Equipment* 830 (2016) 30 – 35. doi:<https://doi.org/10.1016/j.nima.2016.05.030>. URL <http://www.sciencedirect.com/science/article/pii/S016890021630393X>
- [30] S. Agostinelli, et al., Geant4: a simulation toolkit, *Nuclear Instruments and Methods in Physics Research Section A: Accelerators, Spectrometers, Detectors and Associated Equipment* 506 (3) (2003) 250 – 303. doi:[https://doi.org/10.1016/S0168-9002\(03\)01368-8](https://doi.org/10.1016/S0168-9002(03)01368-8). URL <http://www.sciencedirect.com/science/article/pii/S0168900203013688>
- [31] Hamamatsu mppc s13360-6050 datasheet. URL https://www.hamamatsu.com/eu/en/product/optical-sensors/mppc/mppc_mppc-array/S13360-6050PE.html